

## Article

# Effect of Heat Treatment on Microstructure, Tensile Properties and High-Temperature Corrosion Resistance of the FeCrMnNi High Entropy Alloy

Zhen Cai <sup>1</sup>, Na Wei <sup>2,3,\*</sup>, Yaolei Han <sup>1</sup>, Fang Si <sup>4</sup>, Lei Mi <sup>2,3</sup>, Chenhui Zhang <sup>2,3</sup>, Xiaohua Liu <sup>2,3</sup>, Fengyang Jiang <sup>4</sup> and Tiandong Wu <sup>2,3</sup>

<sup>1</sup> Power Station Life Management Technology Center, Suzhou Nuclear Power Research Institute, Suzhou 215004, China

<sup>2</sup> Technology Center, Xi'an Chao Jing Technology Co., Ltd., Xi'an 710200, China

<sup>3</sup> Shanxi Key Laboratory of Advanced Metal Structural Materials Precision Thermoforming, Xi'an 710200, China

<sup>4</sup> School of Materials Engineering, Xi'an Polytechnic University, Xi'an 710048, China

\* Correspondence: nawei0314@163.com; Tel.: +86-187-1046-9475

**Abstract:** FeCrMnNi high-entropy alloys prepared by vacuum induction melting were tested and characterized using an X-ray diffractometer, a scanning electron microscope, a micro hardness tester and a universal tensile tester to investigate the effects of the heat treatment temperature on the microstructure and mechanical properties of the alloys and the heat-resistant corrosion properties of FeCrMnNi alloy after annealing at 800 °C. It is a high-entropy alloy with a typical dendritic (DR) morphology. With the increase in the heat-treatment temperature, the amount of ultrafine precipitates with the BCC structure in the matrix increased; furthermore, the amount of ultrafine precipitates started to decrease at temperatures above 900 °C, and the DR structure gradually weakened. After heat treatment at temperatures above 800 °C, the alloy showed a tensile strength of 721.1 MPa and an elongation at break of 26.7%, which indicates improved strength of the alloy while maintaining good plasticity, mainly because a large amount of nanoscale particles precipitated between the DR structures and enabled fine grain strengthening. Therefore, an appropriate heat-treatment temperature helps to improve the overall mechanical properties of the high-entropy alloy.

**Keywords:** high entropy alloy; heat treatment; microstructure; mechanical properties; high temperature steam corrosion



**Citation:** Cai, Z.; Wei, N.; Han, Y.; Si, F.; Mi, L.; Zhang, C.; Liu, X.; Jiang, F.; Wu, T. Effect of Heat Treatment on Microstructure, Tensile Properties and High-Temperature Corrosion Resistance of the FeCrMnNi High Entropy Alloy. *Metals* **2022**, *12*, 1537. <https://doi.org/10.3390/met12091537>

Academic Editors: Frank Czerwinski and Fei Yang

Received: 5 July 2022

Accepted: 9 September 2022

Published: 16 September 2022

**Publisher's Note:** MDPI stays neutral with regard to jurisdictional claims in published maps and institutional affiliations.



**Copyright:** © 2022 by the authors. Licensee MDPI, Basel, Switzerland. This article is an open access article distributed under the terms and conditions of the Creative Commons Attribution (CC BY) license (<https://creativecommons.org/licenses/by/4.0/>).

## 1. Introduction

Since their introduction, multi-element high-entropy alloys (HEAs) have attracted considerable attention because of their unique structure and properties [1–6]. Unlike conventional alloys, HEAs can be designed by adjusting the alloy composition to obtain simple face-centered cubic (FCC) [7], body-centered cubic (BCC) [8], or hexagonal close-packed (HCP) [9,10] solid-solution crystal structures, but the application of HEAs is limited because of disadvantages such as compositional segregation, cold cracking and shrinkage, and high internal stresses during the casting process [11–14]. Such defects and stress in the internal structure of an HEA can be eliminated and an alloy with excellent structure and properties can be obtained by adopting an appropriate heat treatment process [7,15,16]. In recent years, the effects of heat treatment on the microstructure and mechanical properties of high-entropy alloys have been studied from two aspects [17–20]: Firstly, the phase structure of HEAs is more stable after heat treatment and the disorder degree in the high-entropy alloy HEA system increases with the heat-treatment temperature. Thus, the alloy will exhibit a simpler and more stable phase structure due to the more pronounced high entropy effect after heat treatment. Yeh et al. [21] cast the Co<sub>1.5</sub>CrFeNi<sub>1.5</sub>Ti<sub>0.5</sub> HEA into single crystals by the conventional Bridgeman technique, and the alloy was stable in the  $\gamma'$ (Ni<sub>3</sub>Ti)

phase at 800 °C and formed an unstable phase associated with the  $\eta$  phase at 900–1000 °C. By annealing the as-cast CoCrFeNiTi0.5 alloy, Li Jiang et al. [22] obtained dendrites (DR) containing in approximate equal amounts of Co, Cr, Fe, Ni, and relatively little Ti, and inter dendrites (ID) consisting of (Ni, Ti)-rich phases, (Fe, Cr)-rich phases, and (Co, Ti)-rich phases. Secondly, the second phase of the high-entropy alloy HEA could be precipitated after heat treatment. There are many elements in the high-entropy alloy HEA and each element has a different mixing enthalpy and solid solution degree. Therefore, the elements in the as-cast alloy are distributed in different regions of the microstructure, the elements are distributed in different regions of the microstructure, and the supersaturated elements can be precipitated from the solid solution due to the decrease in the solid solubility with the decrease in the temperature during the cooling stage of heat treatment. In this study, CoCrFeNi [23], CoCrFeMnNi [11], and Al0.1CoCrFeNi alloys [24] were fully recrystallized and annealed, and their mechanical properties were found to have similar characteristics: i.e., good plasticity and low yield strength. Further, the FeCoNiCrMn series of HEAs are the first proposed HEAs with a single-phase FCC structure, which can maintain excellent plasticity and fracture toughness from room temperature to liquid nitrogen temperature. However, the application and development of the alloy as a structural material are seriously limited owing to the presence of the expensive Co element and its low yield strength of less than 200 MPa at room temperature. In order to cope with complex environments such as high temperature, corrosion and vibration, FeCrMnNi HEA should not only have good mechanical properties, but also have excellent heat and corrosion resistance. FeCrMnNi HEA contains a high content of anti-oxidation and anti-corrosion element Cr, so its thermal corrosion resistance is studied.

In this study, we investigated the effect of the heat treatment temperature on the microstructure and mechanical properties of the FeCrMnNi HEA (without Co) and we used the heat treatment method to precipitate the second phase in the alloy in order to improve its comprehensive mechanical properties. In order to explore its application potential in new structural materials its heat and corrosion resistance were investigated.

## 2. Materials and Methods

In this experiment, Fe, Cr, Mn, and Ni metal particles with purity of 99.95% were used to prepare primary ingots by vacuum induction melting, and the compensation amount of Mn was determined to be 5%, by considering the burning loss of Mn during the melting process. Vacuum arc melting was used for secondary melting. The nominal contents of each element in the ingot obtained by vacuum consumable arc melting are shown in Table 1, and the chemical composition results are close to the target values, with the chemical compositions in the head and tail being evenly distributed.

**Table 1.** Elemental ratios for each system of high entropy alloys.

Alloy System	Fe/wt%	Cr/wt%	Mn/wt%	Ni/wt%
FeCrMnNi	25.2	23.5	24.8	26.5

Subsequently, rectangular test samples with the dimensions of 7 mm × 7 mm × 50 mm were cut from the high-entropy alloy ingot by wire electrical discharge machining (WEDM), and the samples were heat-treated at 700 °C, 800 °C, 900 °C, and 1000 °C with the same heating time using a resistance furnace (Baoji De'an Industrial Furnace Co., Ltd., Xi'an, China), followed by air-cooling. These were cut into test samples with the dimensions of 7 mm × 7 mm × 5 mm by WEDM. The as-cast and annealed samples were ground with sandpaper with different particle sizes. Then, diamond was used for polishing until there was no scratch on the surface under the metallographic microscope at 500 times. Finally, the aqua regia was used as the corrosion solution to deal with the surface of the samples. After the surface of the samples was cleaned with alcohol, these samples were used for XRD analysis, microstructure observation, and Vickers hardness test.

The phase structure of the test sample was analyzed by using an Empyrean X-ray diffractometer (XRD, Shimadzu Co., Ltd., Kyoto, Japan), with copper as the diffraction target, a scanning angle of  $20\text{--}100^\circ$ , and a scanning speed of  $5^\circ/\text{min}$ . The microstructure was characterized by using a Quanta-450-FEG + X-MAX50 scanning electron microscope (SEM, Japan Electronics Co., Ltd., Tokyo, Japan), and the elemental composition was analyzed using an energy spectrometer (EDS, Japan Electronics Co., Ltd., Tokyo, Japan). The differential thermal analysis was performed with a Netzsch STA 449 C high-pressure differential scanning calorimeter (NETZSCH Scientific Instruments Trading (Shanghai) Ltd., Shanghai, China). Further, the hardness test was carried out with a HV-10 micro-Vickers hardness tester (Shen Zhen XinAansi material testing Co., Ltd., Shenzhen, China) with a test load force of 200 g and a holding time of 5 s, and the tensile properties were tested by using a universal testing machine.

The FeCrMnNi alloy after heat treatment at  $800^\circ\text{C}$  was subjected to corrosion test in an autoclave. The corrosion solution was 1000 ppm boric acid and 2 ppm lithium hydroxide, and the temperature and pressure were  $360^\circ\text{C}$ , 18 Mpa,  $400^\circ\text{C}$  and 10.3 Mpa respectively. The sampling time is 3 days, 10 days and 14 days. Each sampling was weighed by electronic balance, and the corrosion morphology was observed and analyzed by scanning electron microscope.

### 3. Results and Discussion

#### 3.1. DSC Curve Analysis

The DSC pattern of the FeCrMnNi alloy from room temperature up to  $1200^\circ\text{C}$  is shown in Figure 1. An endothermic peak and an exothermic peak are seen at  $744^\circ\text{C}$  and  $870^\circ\text{C}$ , respectively, indicating a phase change during heating. The absence of a low-temperature peak indicates that no solid-state phase change occurred in the alloy at low temperatures. With increasing temperature, the phase in the alloy changed from the metastable to the stable state, during which the new phase was precipitated and dissolved in the supersaturated FCC solid solution.

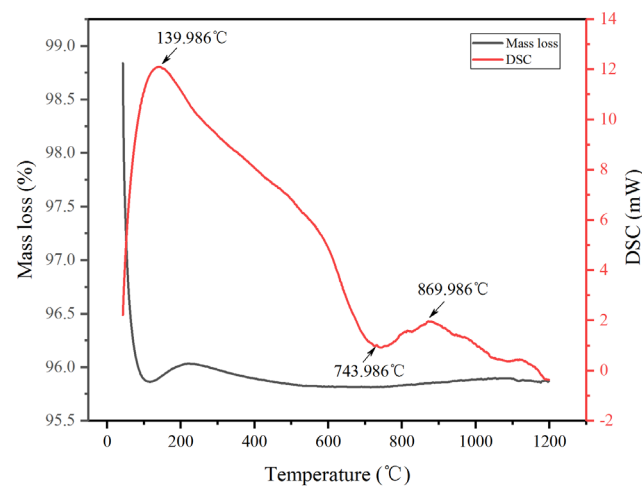


**Figure 1.** DSC pattern for FeCrMnNi alloy.

#### 3.2. Effect of Heat Treatment Temperature on the Phase Structure of FeCrMnNi Alloy

XRD patterns of as-cast FeCrMnNi alloy samples after heat treatment at  $700^\circ\text{C}$ ,  $800^\circ\text{C}$ ,  $900^\circ\text{C}$  and  $1000^\circ\text{C}$  for 2 h are shown in Figure 2a. The main phase is FCC phase for most of the diffraction peaks corresponding to the FeNi alloy (PDF#47-1405) with the FCC phase. Additionally, the (110) crystal plane diffraction peak of BCC phase (PDF#34-0396) was detected. After annealing, the intensity of the BCC-phase diffraction peak at  $2\theta$  of about  $44^\circ$  increased with the annealing temperature and reached the highest at  $800^\circ\text{C}$ , which suggests that the amount of the precipitated BCC phase increased. Furthermore, the intensity of the BCC phase diffraction peak gradually decreased when the annealing temperature was

further increased to 1000 °C and the amount of precipitated BCC phase decreased when the alloy was heat-treated at a higher temperature. The FCC solid solution in the as-cast FeCrMnNi high-entropy alloy was a metastable supersaturated solid solution. When the alloy was treated at an appropriate temperature, the BCC solid-solution phase precipitated from the FCC phase and the FCC phase started to become stable, whereas at higher heat-treatment temperatures, the precipitation of the BCC phase was gradually suppressed. The phase change trends during the heat treatment were basically consistent with the DSC results mentioned above. From the enlarged (111) diffraction peak in Figure 2b, it can be seen that after the heat treatment, the main peak shifted slightly to the right (large angle), indicating that the lattice constant of the FCC phase was reduced and thus the lattice distortion was weakened.

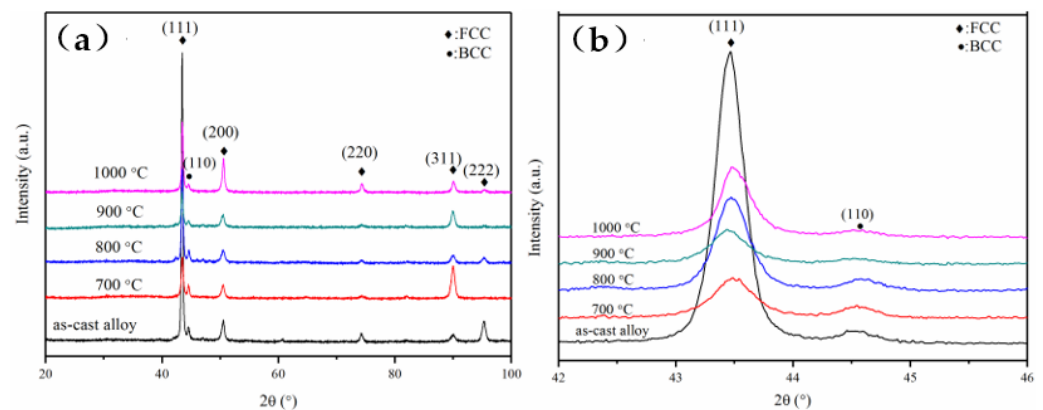


**Figure 2.** XRD patterns of the FeCrMnNi alloys (a) XRD patterns of FeCrMnNi alloys and (b) XRD patterns of FeCrMnNi alloys.

The FeCrMnNi alloy exhibited stable FCC and BCC crystal structures in both as-cast and heat-treated states, and subsequent heat treatment did not result in a phase change. However, the peak intensity ratio of  $I(111)/I(200)$  for the as-cast specimen was significantly higher than that of  $I(111)/I(200)$  in the heat-treated sample, suggesting that texture [25] might be formed in the grains of the as-cast FeCrMnNi high-entropy alloy, which is commonly found in the face-centered high-entropy alloy after plastic deformation. The  $I(111)/I(200)$  peak intensity ratio decreased during the subsequent annealing process, demonstrating a weakening of the (111) texture during the annealing.

According to the Hume–Rothery rules, the atomic size difference ( $\delta$ ) and the enthalpy of mixing ( $\Delta H_{mix}$ ) are the two main factors for predicting the phase formation:

$$\delta = \sqrt{\sum_{i=1}^N c_i \left( 1 - r_i / \left( \sum_{i=1}^N c_i r_i \right) \right)^2} \quad (1)$$

$$\Delta H_{mix} = \sum_{i=1, i \neq j}^N \Delta H_{AB}^{mix} c_i c_j \quad (2)$$

Here,  $N$  is the number of components in the alloy system,  $c_i$  and  $c_j$  are the atomic percentages of the  $i$ -th and  $j$ -th components,  $r_i$  is the atomic radius of the  $i$ -th component, and the mixing enthalpy of the binary equiatomic AB alloy was  $-6.04$  kJ/mol (within the range of  $-15$  to  $5$  kJ/mol) and  $\delta$  was  $2.75\%$  (within the range of  $1$  to  $5\%$ ). In addition, the valence electron concentration (VEC) was used to estimate the stability of the solid solution, and it is defined as follows:

$$VEC = \sum_{i=1}^n c_i (VEC)_i \quad (3)$$

Here,  $c_i$  is the atomic percentage of the  $i$ -th component and  $(VEC)_i$  is the VEC of the  $i$ -th element. The results show that the VEC of the FeCrMnNi alloy was  $7.75$  (within in the

range of 6.87 to 8.0), demonstrating that the mixed FCC phase and BCC phase could exist simultaneously in the FeCrMnNi alloy, which is consistent with the XRD analysis results.

### 3.3. Effect of Heat Treatment Temperature on the Microstructure of FeCrMnNi Alloy

From Figure 3a–e, it can be concluded that the as-cast FeCrMnNi alloy exhibited the typical DR morphology, as seen from the light gray DR and dark gray ID. The grain size of as-cast alloy is 800 nm~200  $\mu$ m. After heat treatment at 700  $^{\circ}$ C, the amount of ID gradually increased. This is mainly because there were a larger number of elements in the alloy and the elements with a high melting point solidified first during the solidification of the alloy; this resulted in the enrichment of the low-melting-point elements in the solidification front, lowered the actual solidification temperature of the liquid phase in front of the solidification interface, and led to component super-cooling. With increasing heat treatment temperature, an increasing number of atoms were released from the supersaturated DR and diffused into the ID region. After heat treatment at 800  $^{\circ}$ C, an increasing amount of precipitated phases were dispersed in the matrix, granular ultrafine precipitates were observed, the amount of coarse DR was significantly reduced, and the structure of the DR was gradually weakened. These observations indicate that with increasing temperature, the diffusion activation energy in the alloy system increased, which accelerated the diffusion migration between atoms and promoted the mutual solubility between elements; thus, the microstructure transformed and the composition became gradually homogenized. The ultrafine precipitated phase might be the BCC structure detected by XRD analysis. After heat treatment at 900  $^{\circ}$ C, the precipitates grew gradually from fine grains to fine needle-like structures, and the area of the ID increased, resulting in the formation of a network structure. With the increase in the heat treatment temperature to 1100  $^{\circ}$ C, the DR disappeared and became island-like independent structures, the amount of precipitates decreased significantly, and the precipitates grew into coarse grains. Thus, heat treatment temperatures higher than 800  $^{\circ}$ C promote the growth of microstructures, resulting in a large number of defects and vacancies in the alloy.

SEM micrographs of the FeCrMnNi alloy samples after heat treatment at 700  $^{\circ}$ C, 800  $^{\circ}$ C, 900  $^{\circ}$ C, and 1000  $^{\circ}$ C are shown in Figure 3(b1)–(e1). After heat treatment at 700  $^{\circ}$ C, the precipitates were fine needles with lengths ranging from a few hundred nanometers to about 10  $\mu$ m. When the alloy sample was treated at 800  $^{\circ}$ C, the precipitates in the region close to the ID were larger and were granular or rod-shaped, and the precipitates away from the ID were fine nanoscale granular structures. Furthermore, the ultra-fine precipitates of the sample treated at 800  $^{\circ}$ C were more dispersed than those of the sample treated at 700  $^{\circ}$ C. The precipitates of the alloy samples treated at 900  $^{\circ}$ C and 1000  $^{\circ}$ C grew larger and decreased in number with increasing heat treatment temperature, suggesting that the formation of precipitates was suppressed with the increase in the temperature, which is consistent with the results of XRD analysis.

The image obtained after heat treatment at 1000  $^{\circ}$ C is enlarged and shown in Figure 3e. Obvious twin morphologies are visible, which can be attributed to the following: Twins tend to occur in some metals or alloys whose lattice structure is mainly FCC, and FeCrMnNi high-entropy alloys are mainly composed of the FCC phase. The atoms in FeCrMnNi alloys can diffuse sufficiently and form new phases after high-temperature and long-duration heat treatment, and twins are formed during the formation and growth of new phases. The growth of a new phase is accompanied by the movement of the phase boundary, during which the atomic layers on the (111) crystal plane at the phase boundary corner (111) occasionally appears to be mis-stacked, resulting in the appearance of a total lattice of twin boundaries, followed by the formation of twins at the phase boundary corner. The appearance of twins indicates that the higher temperature is sufficient to overcome the stacking fault energy to form twins [26,27], which can result in grain refinement of the coarse grains, thereby improving the overall alloy mechanical properties.

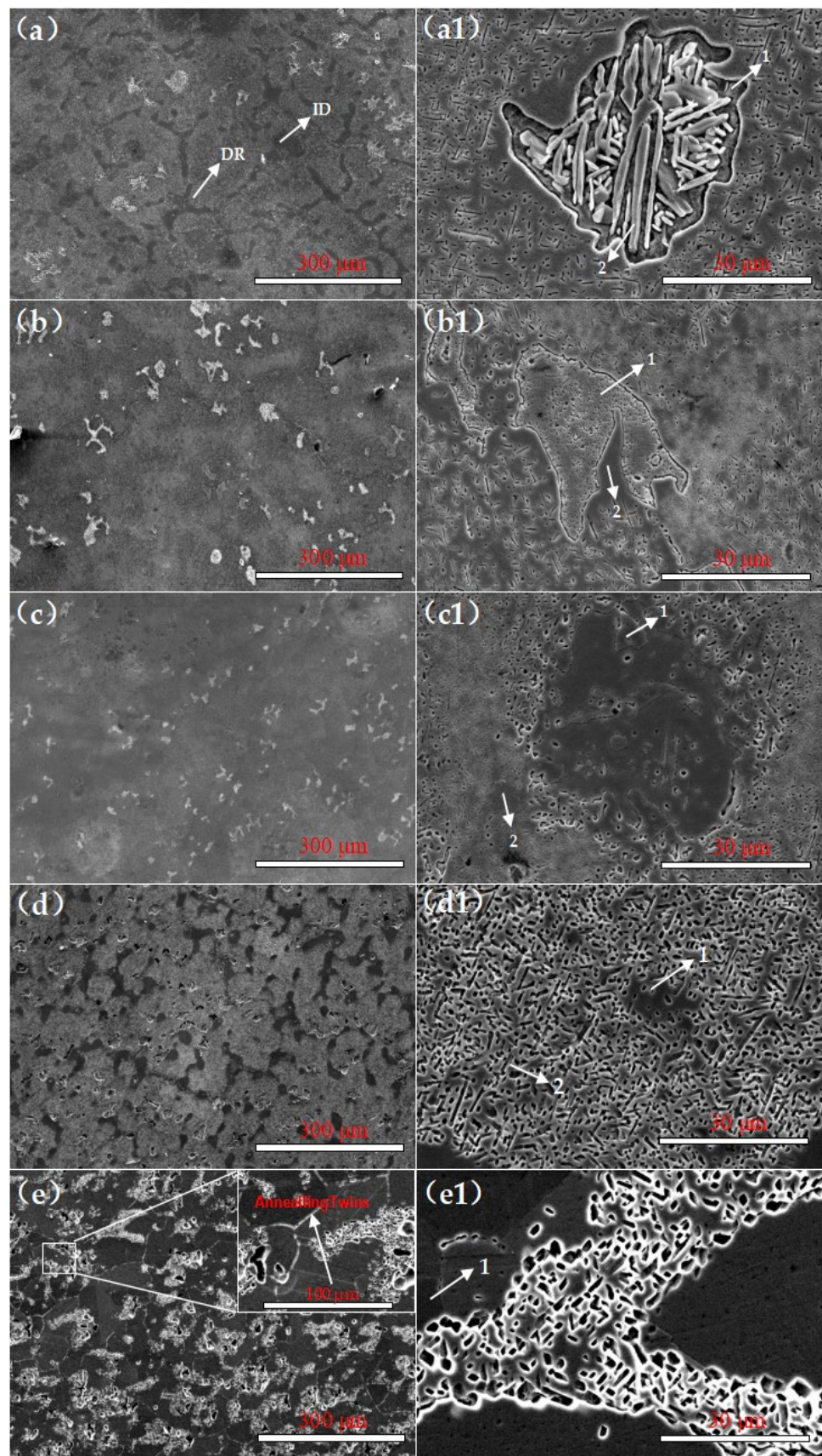


**Figure 3.** Microstructure and morphology of cast FeCrMnNi alloys and after heat treatment (a,a1) as-cast (b,b1) 700 °C (c,c1) 800 °C (d,d1) 900 °C (e,e1) 1000 °C.

Element planes scans were performed for Figure 3(a1,b1,d1), and the element distribution is shown in Figure 4. There were Cr-rich and Ni-poor zones in the FeCrMnNi alloy in the as-cast state and after heat treatment at 700 °C, with uniform distribution of Fe and Mn. When the heat treatment temperature was increased to 900 °C, the distribution of Fe, Cr, Mn, and Ni gradually tended to become uniform. The areas corresponding to the points marked (1 and 2) in Figure 3 were analyzed through EDS point scanning, and the elemental contents at each point are listed in Table 2. The results show that the elemental content of the matrix was basically in accordance with the designed composition of this alloy. Further, in the as-cast alloy sample, and samples heat-treated at 700 °C and 800 °C, segregation of Cr occurred at the position of the precipitated second phase, and the precipitated second phase could be identified as the FeCr phase with the BCC structure. In the alloy samples heat-treated at 900 °C and 1000 °C, the elemental contents were basically consistent with the designed composition of the alloy, indicating that the higher heat treatment temperature is conducive to further homogenization of the alloy composition.

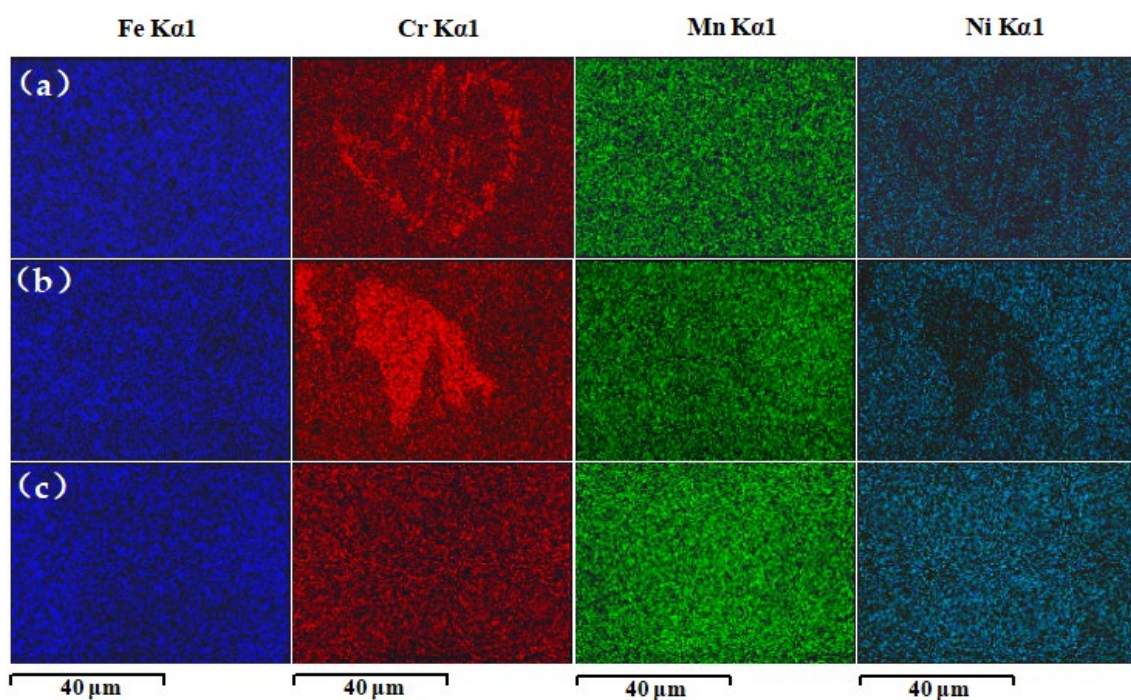


**Figure 4.** Elemental distribution pattern of as-cast and heat treated FeCrMnNi alloys (a) as-cast (b) heat-treated at 700 °C (c) heat-treated at 900 °C.

**Table 2.** EDS analysis results of FeCrMnNi alloy micro-zones shown in Figure 3.

State of Test Sample	Position	Fe/At%	Cr/At%	Mn/At%	Ni/At%	C/At%
As-cast	1	28.13	42.70	14.56	8.63	5.97
	2	29.88	25.76	16.90	20.59	6.88
Heat-treated at 700 °C	1	28.03	39.36	16.27	11.78	4.56
	2	28.49	20.86	20.97	24.39	5.29
Heat-treated at 800 °C	1	28.78	42.87	13.84	10.10	4.41
	2	18.90	15.15	28.13	34.25	3.57
Heat-treated at 900 °C	1	27.85	18.80	21.32	26.47	5.55
	2	28.14	18.97	21.94	26.28	4.68
Heat-treated at 1000 °C	1	26.72	21.55	20.71	24.16	6.86

### 3.4. Effect of Heat Treatment Temperature on Mechanical Properties of FeCrMnNi Alloy

The variation in the micro-hardness of FeCrMnNi alloy at different heat treatment temperatures is shown in Figure 5. The micro-hardness of the alloy decreases as the

temperature increases, with the fastest decrease in hardness occurring at 900 °C and 1000 °C, mainly due to the recrystallization of the alloy in this temperature range.

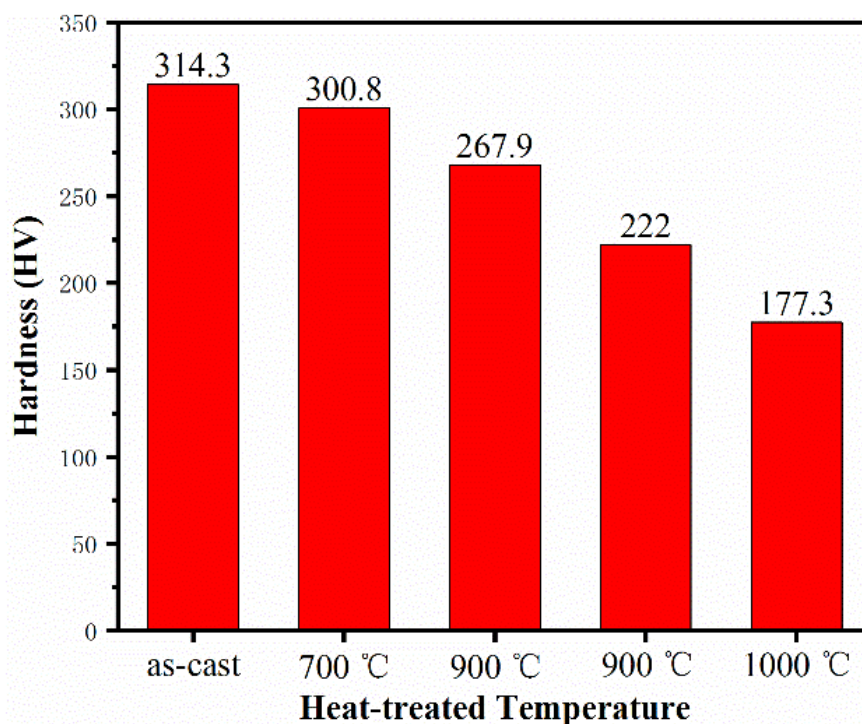


**Figure 5.** Micro-hardness of FeCrMnNi alloy at different heat treatment temperatures.

The tensile stress–strain curves of the as-cast and heat-treated FeCrMnNi alloys are shown in Figure 6. The as-cast FeCrMnNi alloy had a yield strength of 557.1 MPa, a tensile strength of 717.2 MPa, and an elongation at break of 24.6% as shown in Table 3. The tensile strengths of the FeCrMnNi high-entropy alloy samples after heat treatment at 700 °C and 800 °C were 696.2 MPa and 719.2 MPa, respectively, i.e., very similar to the value for the as-cast alloy. After heat treatment at 700 °C, the elongation at break of the alloy decreased significantly and the plastic fracture. The elongation at break increased slightly after heat treatment at 800 °C, mainly because more nanoscale particles were precipitated between the DR, and this played a role in grain refinement and could be inferred to result in excellent overall mechanical properties according to the Hall–Petch theory. After heat treatment at 900 °C and 1000 °C, the tensile strength of the FeCrMnNi alloy decreased, but it had significantly increased elongation at break and highest plasticity after heat treatment at 1000 °C; this was mainly because of a large number of microcracks at the grain boundaries of the sample heat-treated at 1000 °C, which is more favorable to the dislocation slip, and can effectively improve the plasticity of the alloy, resulting in the highest plasticity of the alloy treated at this temperature. In addition, it is also possible that there are a higher number of FCC structures with better shaping properties, which also confirms the accuracy of the XRD analysis results.

**Table 3.** Tensile properties of FeCrMnNi alloy heat-treated at different temperatures.

Test Sample	Elongation at Break (%)	Tensile Strength (MPa)	Yield Strength (MPa)
As-cast	24.6	717.2	557.1
Heat-treated at 700 °C	13.5	696.2	623.7
Heat-treated at 800 °C	26.7	719.2	589.0
Heat-treated at 900 °C	14.6	568.6	447.1
Heat-treated at 1000 °C	51.1	661.2	243.4

According to XRD analysis results, when the heat treatment temperature was increased to 700 °C, the amount of precipitating BCC phase increased and the slip plane was the (110) plane, which makes it difficult to be activated, and due to the low stacking fault energy and high stacking fault probability of BCC, the dislocation plugging was not easily relieved, thus it was of high tensile and poor toughness. In case of heat treatment at 1000 °C, the crystal structure of the alloy was FCC + BCC, and the amount of the FCC phase increased with increasing temperature. Further, the slip plane of the FCC crystal structure was the (111) plane, and the slip system could be easily activated, which results in the excellent plasticity of the alloy sample.

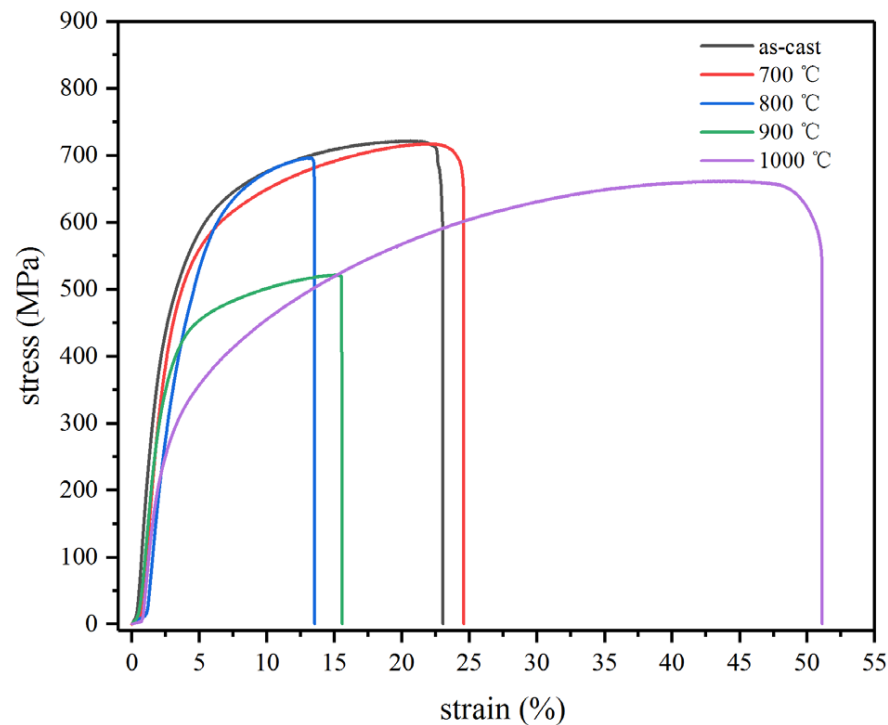


**Figure 6.** Tensile stress-strain curve of FeCrMnNi alloys.

The SEM images of tensile fracture of as-cast and heat-treated FeCrMnNi alloy samples are shown in Figure 7. The fracture morphology of the as-cast sample was mainly characterized by ductile dimple fracture and some flat cleavage fracture. After heat treatment at 700 °C and 800 °C, there were a large number of dimples and a few tearing ridges on the fracture surface. According to the SEM images, the FeCrMnNi alloy was composed of the FCC and BCC phases; furthermore, there were a large number of dimples in the FCC phase region, and in the BCC phase region, there were a few tearing ridges but not obvious dimples. For treatment at 900 °C, the alloy was characterized by intergranular fracture, while dimples still could be observed in the grains. Thus, from the XRD and SEM microstructure results, after treatment at 900 °C, the BCC phase changed into the FCC phase. Further, BCC was a brittle phase at grain boundaries, resulting in the brittle hard phase at grain boundaries to be the crack source during tensile deformation. With the increase in the deformation stress, the cracks expanded along the grain boundaries until fracture.

### 3.5. Hot Corrosion Properties of FeCrMnNi Alloy

#### 3.5.1. Corrosion Weight Loss Curve

Figure 8 shows the weight loss curves of corrosion samples of FeCrMnNi alloy and zirconium alloy at 360 °C and 400 °C, respectively. It can be seen from Figure 8a that FeCrMnNi loses weight in 360 °C high temperature and high pressure water environment, while zirconium alloy gains weight. With the increase in corrosion time, the weight loss of

FeCrMnNi did not change significantly, and the weight gain of zirconium alloy increased. As can be seen from Figure 8b, in the high-temperature steam environment at 400 °C, FeCrMnNi loses weight first, then gains weight, and the weight increase increases with time. The weight gain of zirconium alloy increases with time.

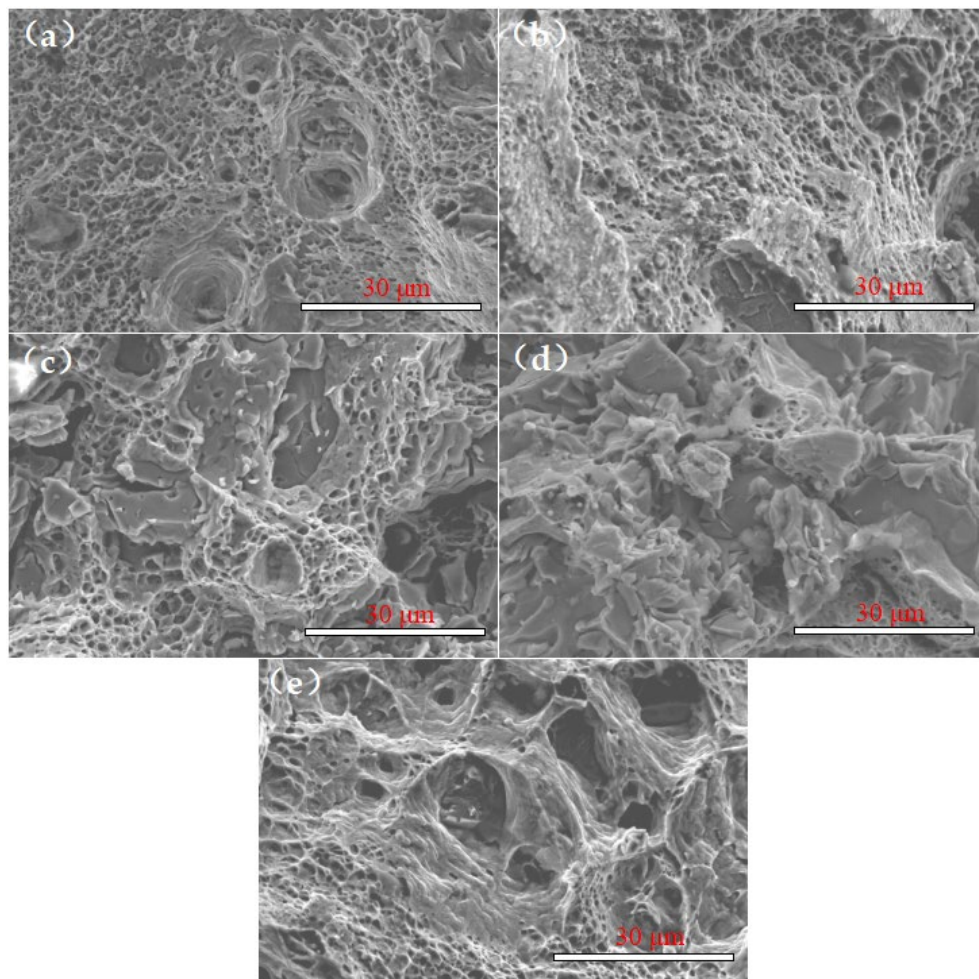


Figure 7. Tensile fracture morphology of as-cast and heat-treated FeCrMnNi alloys (a) as-cast, (b) 700 °C, (c) 800 °C, (d) 900 °C, (e) 1000 °C.

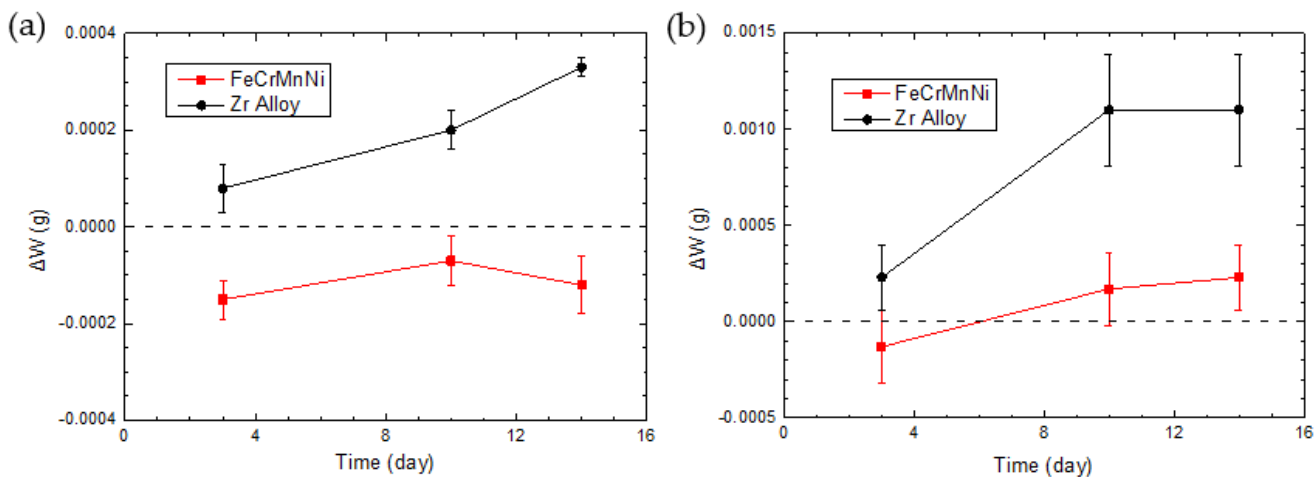
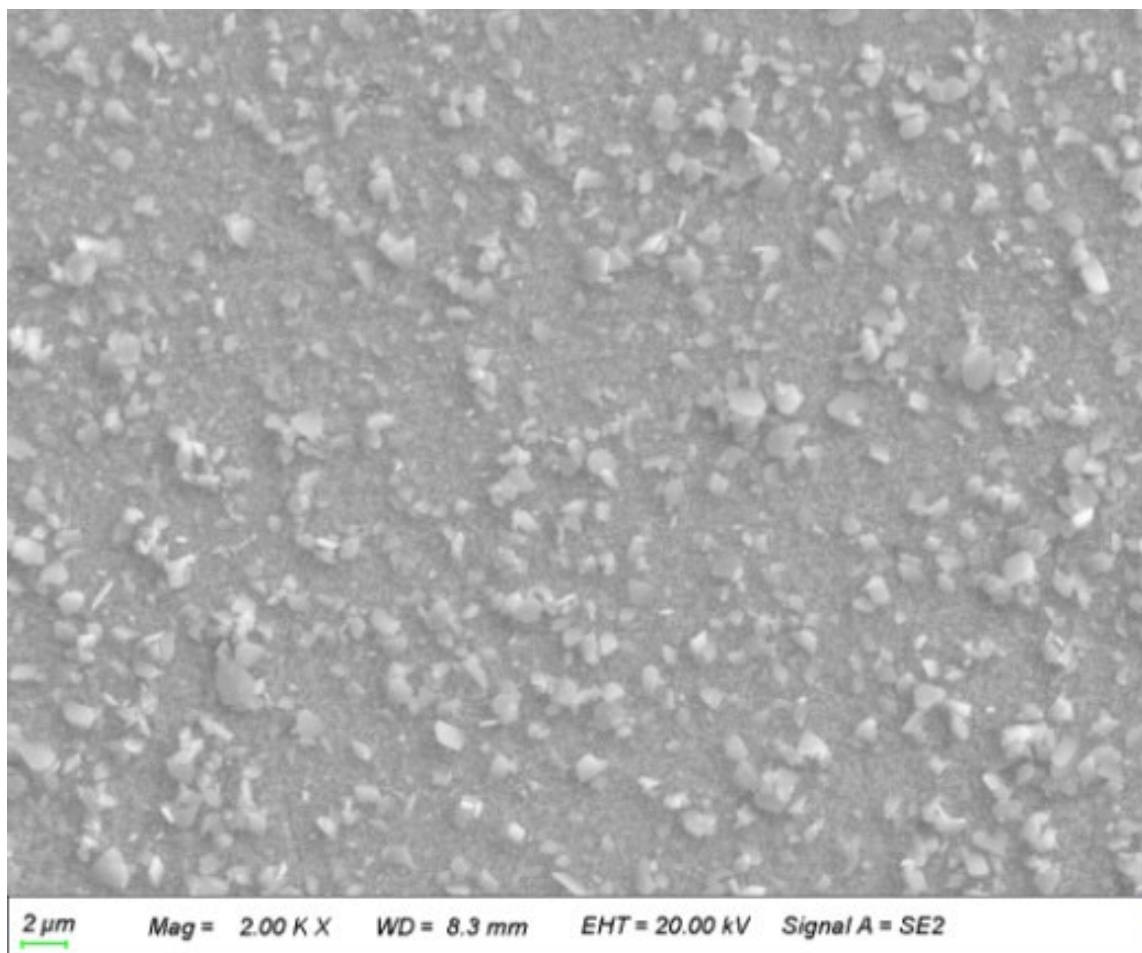


Figure 8. Corrosion weight loss curve of FeCrMnNi alloy (a) 360 °C (b) 400 °C.

### 3.5.2. Hot Corrosion Morphology

Figure 9 shows the microstructure of FeCrMnNi after corrosion in 360 °C high temperature and high pressure water environment for 14 days. More evenly distributed oxide particles are formed on the surface of FeCrMnNi. Through the surface scan analysis of the distribution of O, Fe, Cr, Mn and Ni contents, as shown in Figure 10, it can be seen that the oxygen content of large particles is high and the oxygen content of the substrate is low, while the composition difference of Fe, Cr, Mn and Ni cannot be seen, so it needs further point scan analysis. There is no obvious corrosion product on the surface of zirconium alloy. It can be seen that the composition is evenly distributed and there is no element aggregation. According to the composition analysis, as shown in Figure 11, the content of O, Zr, Sn, Fe and Cr is 29.4 wt.%, 69.3 wt.%, 1.0 wt.%, 0.2 wt.% and 0.1 wt.%, respectively.



**Figure 9.** Microstructure after corrosion in 360 °C high temperature and high pressure water environment for 14 days of FeCrMnNi alloy.

Table 4 shows the results of point component analysis of Figure 11. It can be seen from the composition analysis results in Table 4 that the outer layer of FeCrMnNi alloy has large particles, high oxygen content, mainly Fe and Cr oxides, and low Ni content. The oxygen content of small particles is about half lower than that of large particles, the content of Fe and Cr increases, and the content of Ni increases slightly. The oxygen content of the bottom layer is the lowest, and Fe, Cr and Ni are slightly higher than those of small particles. The content of Mn is small and basically the same in the three morphologies.

**Table 4.** Spot scan composition of FeCrMnNi alloy after corrosion in 360 °C high temperature and high pressure water environment for 14 days.

Position	Analysis Point	O	Fe	Cr	Mn	Ni
Large Particle	29	28.8	51.1	14.8	0.9	4.5
Large Particle	30	27.6	52.0	14.6	1.0	4.9
Granule	31	15.2	60.4	16.8	0.9	6.8
Granule	32	15.2	61.1	16.3	0.9	6.5
Base	33	9.4	65.2	17.6	0.9	6.9
Base	34	9.1	65.1	17.8	1.0	7.1

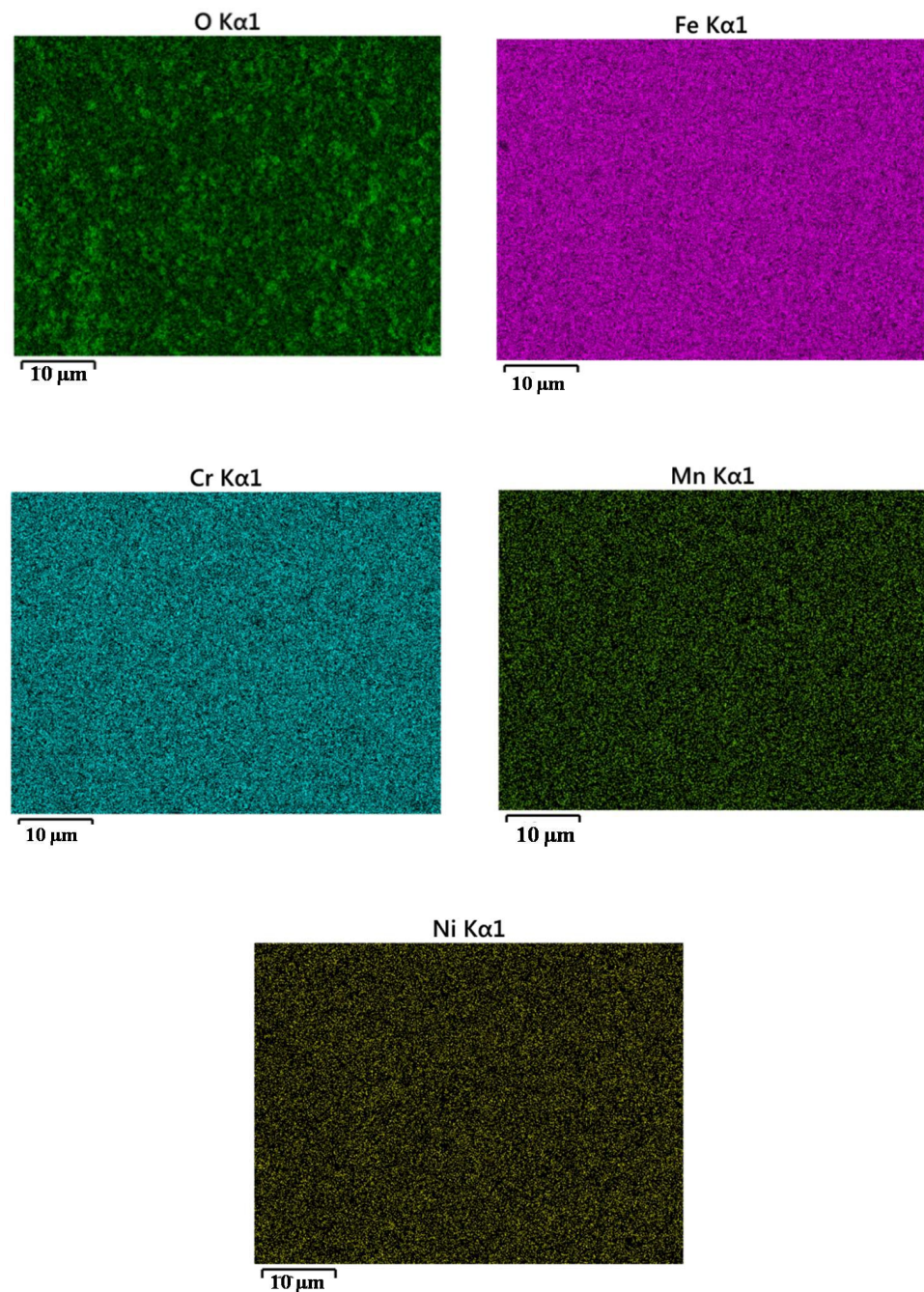


**Figure 10.** Surface scan of FeCrMnNi alloy after corrosion in 360 °C high temperature and high pressure water environment for 14 days.

Figure 12 shows the microstructure of FeCrMnNi after corrosion in 400 °C high temperature and high pressure water environment for 14 days. In 400 °C high temperature and high pressure steam environment, relatively uniform particles are distributed on the surface of FeCrMnNi. It can be seen from the surface scan of Figure 13 that the oxygen content of large particles is high, the oxygen content of substrate is low, and the distribution of Fe, Cr, Mn and Ni is relatively uniform.

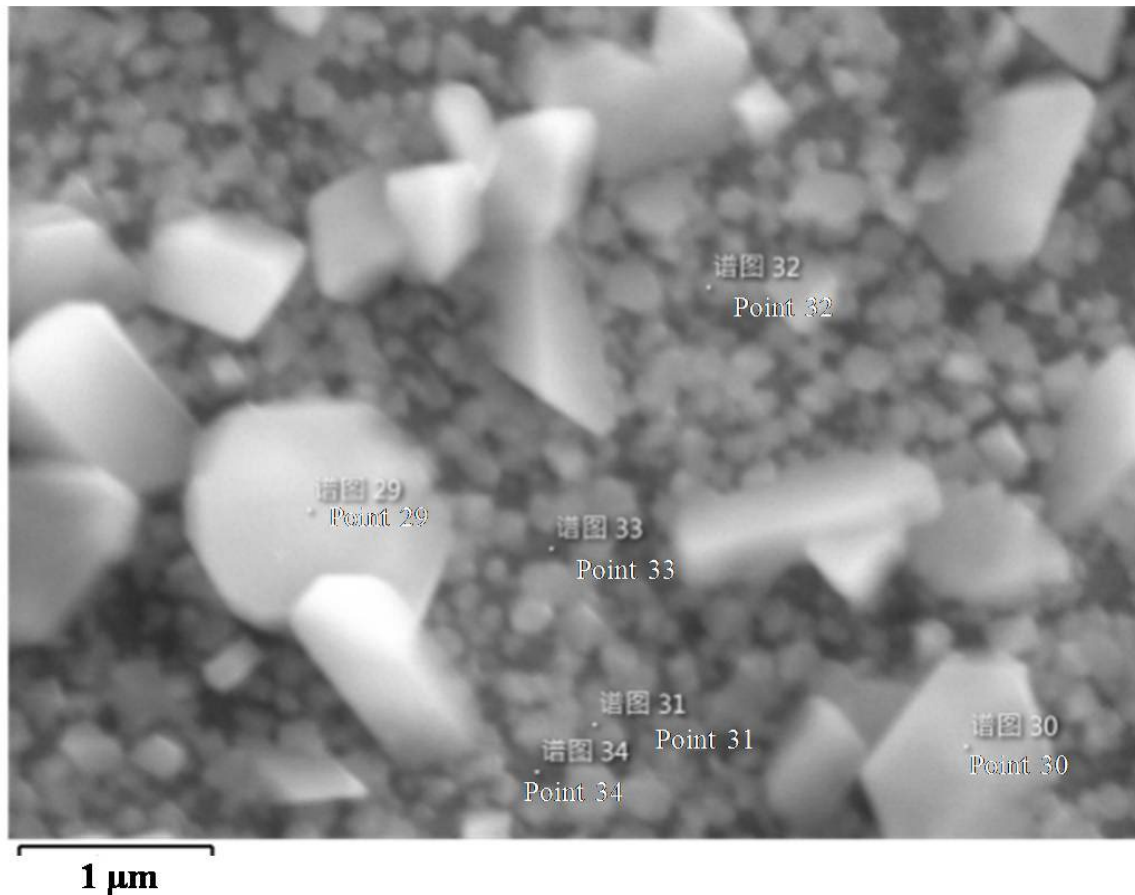


**Figure 11.** Spot scan of FeCrMnNi alloy after corrosion in 360 °C high temperature and high pressure water environment for 14 days.

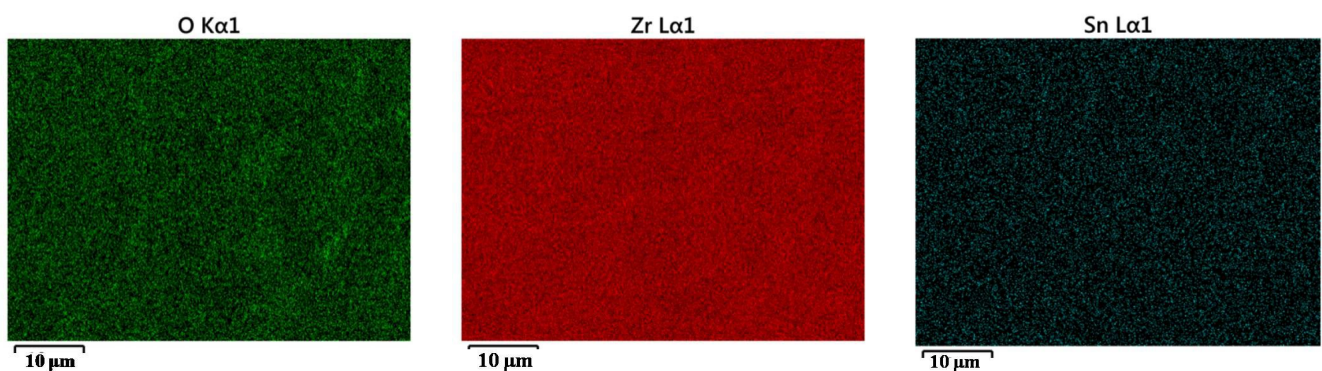


**Figure 12.** Microstructure after 14 days of corrosion in 400 °C high temperature and high pressure water environment of FeCrMnNi alloy.

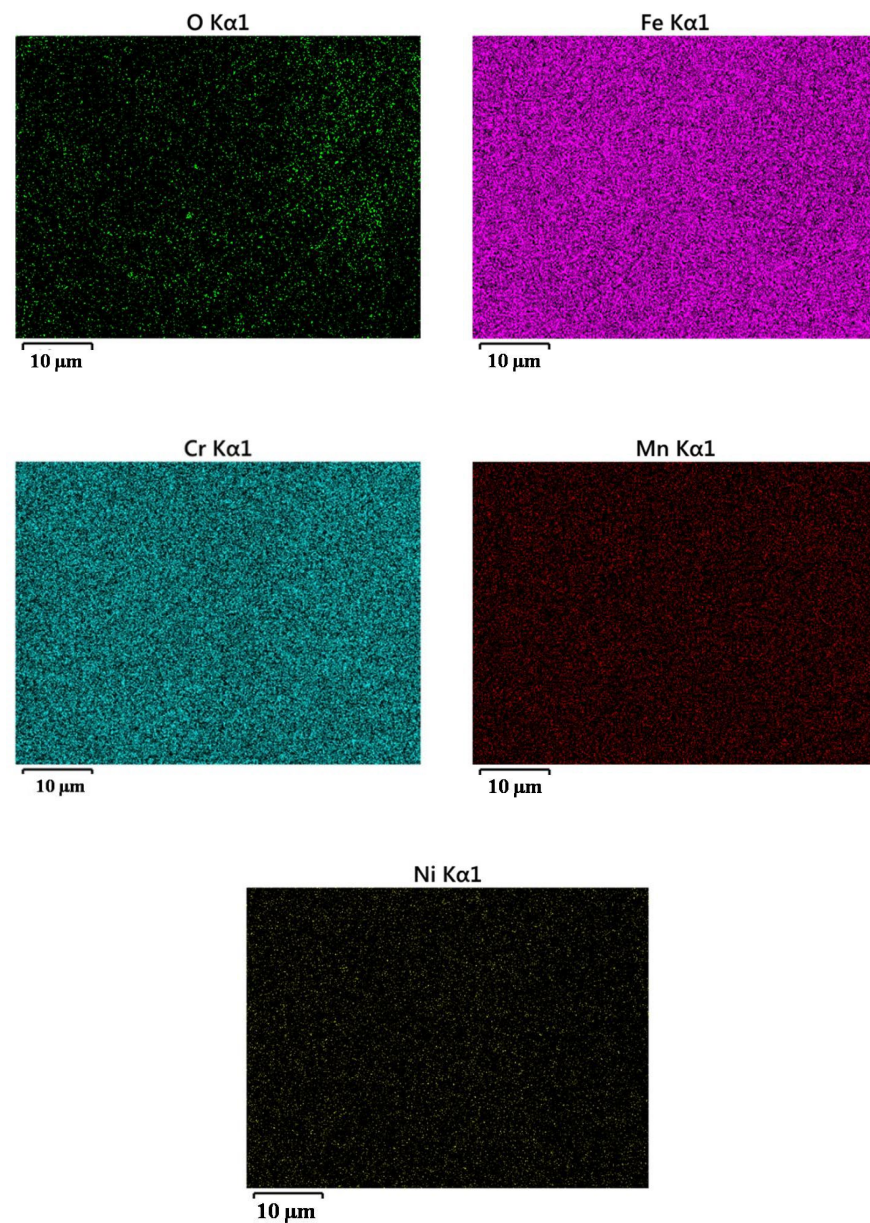


**Figure 13.** Surface scan of FeCrMnNi alloy after corrosion in 400 °C high temperature and high pressure water environment for 14 days.

#### 4. Conclusions

- (1) The FeCrMnNi alloy prepared by the vacuum induction melting method are FCC + BCC two-phase solid solutions, and the FCC solid solution in the as-cast FeCrMnNi high-entropy alloys is a metastable supersaturated solid solution. At an appropriate heat treatment temperature, the BCC solid solution phase precipitated from the FCC phase and the FCC phase began to become stable. At higher heat treatment temperatures, the precipitation of the BCC phase was gradually suppressed.
- (2) The as-cast FeCrMnNi alloy exhibits the typical morphology of DR and the amount of the precipitation phase of the matrix BCC structure increases with the increase in the heat-treatment temperature. After treatment at 800 °C, the ultrafine precipitates were dispersed in the matrix and precipitated, the fine needle-like structure of micro-scale transformed into the granular structure of nano-scale, and the coarse DR of the alloy decreased significantly. After the heat treatment temperature was increased to 900 °C, the amount of ultrafine precipitates began to decrease and the structure of DR weakened gradually. Further, when the heat-treatment temperature

was increased to 1000 °C, the second phase structure became passivated and obvious twin morphology appeared.

- (3) With increasing heat treatment temperature, the tensile strength of the FeCrMnNi alloy showed little change. After heat treatment at 800 °C, the alloy had tensile strength of 721.1 MPa and the elongation at break was 26.7%, which indicates improved strength while maintaining good plasticity. This was mainly because a large number of nanoscale particles precipitated between the DR, resulting in fine crystal strengthening.
- (4) FeCrMnNi alloy loses weight in 360 °C high temperature and high pressure water environment, and the corrosion loss is not obvious with the increase in corrosion time. Evenly distributed oxide particles are formed on the surface, mainly Fe and Cr oxides. After corrosion in 400 °C high temperature and high pressure water environment, it loses weight first and then gains weight. With the increase in corrosion time, the corrosion weight increases obviously, and evenly distributed oxide particles are also formed on the surface. However, the particle size is smaller than that after corrosion at 360 °C, indicating that the heat-resistant corrosion performance of FeCrMnNi at 400 °C is worse than that at 360 °C.

**Author Contributions:** Conceptualization, Z.C.; methodology, F.S.; validation, N.W. and L.M.; formal analysis, Y.H.; investigation, C.Z.; resources, X.L.; data curation, F.J.; writing—original draft preparation, F.S.; writing—review and editing, F.J.; project administration, T.W. All authors have read and agreed to the published version of the manuscript.

**Funding:** This research was funded by the natural science foundation of Jiangsu province (Grants No BK2018021).

**Institutional Review Board Statement:** Not applicable.

**Informed Consent Statement:** Not applicable.

**Data Availability Statement:** Not applicable.

**Acknowledgments:** The authors are grateful for the support provided by The Natural Science Foundation of Jiangsu Province and Shanxi Key Laboratory of Advanced Metal Structural Materials Precision Thermoforming.

**Conflicts of Interest:** The authors declare no conflict of interest.

## References

1. Yeh, J.W.; Chen, S.K.; Lin, S.J.; Gan, J.Y.; Chin, T.S.; Shun, T.T.; Tsau, C.H.; Chang, S.Y. Nanostructured high-entropy alloys with multiple principal elements: Novel alloy design concepts and outcomes. *Adv. Eng. Mater.* **2004**, *6*, 299–303. [[CrossRef](#)]
2. Juan, C.C.; Tsai, M.H.; Tsai, C.W.; Lin, C.M.; Wang, W.R.; Yang, C.C.; Chen, S.K.; Lin, S.J.; Yeh, J.W. Enhanced mechanical properties of HfMoTaTiZr and HfMoNbTaTiZr refractory high-entropy alloys. *Intermetallics* **2015**, *62*, 76–83. [[CrossRef](#)]
3. Tsai, K.Y.; Tsai, M.H.; Yeh, W. Sluggish diffusion in Co-Cr-Fe-Mn-Ni high-entropy alloys. *Acta Mater.* **2013**, *61*, 4887–4897. [[CrossRef](#)]
4. Ranganathan, S. Alloyed pleasures: Multimetallic cocktails. *Curr. Sci.* **2003**, *85*, 1404–1406.
5. Senkov, O.N.; Scott, J.M.; Senkova, S.V.; Meisenkothen, F.; Miracle, D.B.; Woodward, C.F. Microstructure and elevated temperature properties of a refractory TaNbHfZrTi alloy. *J. Mater. Sci.* **2012**, *47*, 4062–4074. [[CrossRef](#)]
6. Xu, Z.Y. *Thermodynamics of Materials*, 4th ed.; Higher Education Press: Beijing, China, 2009; pp. 215–220.
7. Wu, Z.; Bei, H.; Otto, F.; Pharr, G.M.; George, E.P. Recovery, recrystallization, grain growth and phase stability of a family of FCC-structured multi-component equiatomic solid solution alloys. *Intermetallics* **2014**, *46*, 131–140. [[CrossRef](#)]
8. Yeh, J.W.; Lin, S.J.; Chin, T.S.; Gan, J.Y.; Chen, S.K.; Shun, T.T.; Tsau, C.H.; Chou, S.Y. Formation of simple crystal structures in Cu-Co-Ni-Cr-Al-Fe-Ti-V alloys with multiprincipal metallic elements. *Metall. Mater. Trans. A* **2004**, *35*, 2533–2536. [[CrossRef](#)]
9. Feuerbacher, M.; Heidelmann, M.; Thomas, C. Hexagonal high-entropy alloys. *Mater. Res. Lett.* **2015**, *3*, 1–6. [[CrossRef](#)]
10. George, E.P.; Raabe, D.; Ritchie, R.O. *High-Entropy Alloys*; Springer International Publishing: Cham, Switzerland, 2016.
11. Otto, F.; Dlouhý, A.; Somsen, C.; Bei, H.; Eggeler, G.; George, E.P. The influences of temperature and microstructure on the tensile properties of a CoCrFeMnNi high-entropy alloy. *Acta Mater.* **2013**, *61*, 5743–5755. [[CrossRef](#)]
12. Gludovatz, B.; Hohenwarter, A.; Catoor, D.; Chang, E.H.; George, E.P.; Ritchie, R.O. A fracture-resistant high-entropy alloy for cryogenic applications. *Science* **2014**, *345*, 1153–1158. [[CrossRef](#)]
13. Zhang, Y.; Zhou, Y.J.; Lin, J.P.; Chen, G.L.; Liaw, P.K. Solid-solution phase formation rules for multi-component alloys. *Adv. Eng. Mater.* **2008**, *10*, 534–538. [[CrossRef](#)]

14. Guo, S.; Ng, C.; Lu, J.; Liu, C.T. Effect of valence electron concentration on stability of fcc or bcc phase in high entropy alloys. *J. Appl. Phys.* **2011**, *109*, 103505. [[CrossRef](#)]
15. Takeuchi, A.; Inoue, A. Classification of bulk metallic glasses by atomic size difference, heat of mixing and period of constituent elements and its application to characterization of the main alloying element. *Mater. Trans.* **2005**, *46*, 2817–2829. [[CrossRef](#)]
16. Qin, G.; Chen, R.; Liaw, P.K.; Gao, Y.; Wang, L.; Su, Y.; Ding, H.; Guo, J.; Li, X. An as-cast high-entropy alloy with remarkable mechanical properties strengthened by nanometer precipitates. *Nanoscale* **2020**, *12*, 3965–3976. [[CrossRef](#)]
17. Kamikawa, N.; Sato, K.; Miyamoto, G.; Murayama, M.; Sekido, N.; Tsuzaki, K.; Furuhashi, T. Stress-strain behavior of ferrite and bainite with nano-precipitation in low carbon steels. *Acta Mater.* **2015**, *83*, 383–396. [[CrossRef](#)]
18. Yang, T.; Zhao, Y.L.; Luan, J.H.; Han, B.; Wei, J.; Kai, J.J.; Liu, C.T. Nanoparticles-strengthened high-entropy alloys for cryogenic applications showing an exceptional strength-ductility synergy. *Scr. Mater.* **2019**, *164*, 30–35. [[CrossRef](#)]
19. Hou, J.; Zhang, M.; Ma, S.; Liaw, P.K.; Zhang, Y.; Qiao, J. Strengthening in Al<sub>0.25</sub>CoCrFeNi high-entropy alloys by cold rolling. *Mater. Sci. Eng. A* **2017**, *707*, 593–601. [[CrossRef](#)]
20. Bian, B.B.; Guo, N.; Yang, H.J.; Guo, R.P.; Yang, L.; Wu, Y.C.; Qiao, J.W. A novel cobalt-free FeMnCrNi medium-entropy alloy with exceptional yield strength and ductility at cryogenic temperature. *J. Alloy Compd.* **2020**, *827*, 153981. [[CrossRef](#)]
21. Yeh, A.C.; Chang, Y.J.; Tsai, C.W.; Wang, Y.C.; Yeh, J.W.; Kuo, C.M. On the solidification and phase stability of a Co-Cr-Fe-Ni-Ti high-entropy alloy. *Metall. Mater. Trans. A* **2014**, *45*, 184–190. [[CrossRef](#)]
22. Jiang, L.; Lu, Y.; Dong, Y.; Wang, T.; Cao, Z.; Li, T. Annealing effects on the microstructure and properties of bulk high-entropy CoCrFeNiTi<sub>0.5</sub> alloy casting ingot. *Intermetallics* **2014**, *44*, 37–43. [[CrossRef](#)]
23. Wu, Z.; Bei, H.; Pharr, G.M.; George, E.P. Temperature dependence of the mechanical properties of equiatomic solid solution alloys with face-centered cubic crystal structures. *Acta Mater.* **2014**, *81*, 428–441. [[CrossRef](#)]
24. Wu, S.W.; Wang, G.; Yi, J.; Jia, Y.D.; Hussain, I.; Zhai, Q.J.; Liaw, P.K. Strong grain-size effect on deformation twinning of an Al<sub>0.1</sub>CoCrFeNi High-Entropy Alloy. *Mater. Res. Lett.* **2017**, *5*, 276–283. [[CrossRef](#)]
25. Tang, Q.; Huang, Y.; Cheng, H.; Liao, X.; Langdon, T.G.; Dai, P. The effect of grain size on the annealing-induced phase transformation in an Al<sub>0.3</sub>CoCrFeNi High Entropy Alloy. *Mater. Des.* **2016**, *105*, 381–385. [[CrossRef](#)]
26. Cui, Z.Q.; Wang, K.L.; Wu, R. *Metallurgy and Heat Treatment*; Peking University Press: Beijing, China, 2010; pp. 314–322.
27. Gali, A.; George, E.P. Tensile properties of high-and medium-entropy alloys. *Intermetallics* **2013**, *39*, 74–78. [[CrossRef](#)]